Improving the Nonlinear Control Performance of the Supply Fan at Air Handling Units using a Gain Scheduling Control Strategy

Zufen Wang*[1], Rodney Hurt[2], Li Song[2], Gang Wang[1]

1. Department of Civil, Architectural and Environmental Engineering, University of Miami, Coral Gables, FL 33146, USA
2. School of Aerospace and Mechanical Engineering, University of Oklahoma, Norman, OK 73019, USA

*Corresponding author: Phone: 305.284.5555; Fax: 305.284.3492; Email: g.wang2@miami.edu

Abstract

Due to its nonlinear nature, the supply fan at air handling units with the controller tuned at the design condition tends to be aggressive and oscillate under partial load conditions. The objective of this paper is to develop and validate a gain scheduling control strategy to improve its nonlinear control performance. First, a control-oriented model, which does not require numerous physical parameters and extensive test data, is developed to study the nonlinearity of the fan system. Based on the theoretical model and experimental verifications, the issue of an aggressive response with a conventional fixed-gain controller is caused by the fact that the system gain is proportional to the ratio of the duct static pressure to the fan speed. To address the issue, a scheduling function of the measurable duct static pressure and fan speed is proposed to be included in the conventional fixed-gain controller to compensate for the fan system gain variation. The gain scheduling control strategy is found to approximately maintain the identical control performance under all operation conditions. Most

importantly, the gain scheduling control strategy can be readily implemented without intensive computation and additional measurements, showing a promising potential in industrial applications.

1. Introduction

Ventilation energy, which is mainly consumed by the fans in heating, ventilation and air-conditioning systems, accounts for approximately 15.9% of the electricity consumption in commercial buildings in the U.S. (DOE 2011, Zhou, Harberl et al. 2017). Variable air volume (VAV) systems, with adjustable supply fan speed, have gained popularity at air handling units (AHUs) because of their potential to help achieve energy efficiency.

Traditionally, the supply fan speed control system at AHUs is a single control loop system in which the supply fan speed is modulated by the variable frequency drive (VFD) to maintain the duct static pressure setpoint. A nonlinear relationship among the fan speed, airflow rate, and duct static pressure has been identified in numerous experiments (Zaheer-Uddin and Zheng 1994, Mei and Levermore 2002, Wang and Wang 2008), indicating a nonlinear feature of the fan speed control system. On the other hand, the duct static pressure reset in VAV systems has proved to be energy efficient with an energy savings of 30%-50% by supply fans compared with the constant static pressure control strategy (Taylor 2007, Shim, Song et al. 2014) and is required for systems with direct digital control (DDC) at the zone level (ASHRAE 2010). As a result, the dynamical reset of static pressure setpoints will significantly change the fan operation conditions. Moreover, the increasing deployment of occupancy sensors in commercial buildings increases the dynamical reset of the terminal box (TB) minimum airflow setpoints (Esrafilian-Najafabadi and Haghighat 2021), resulting in dynamically variable TB damper positions.

Variable TB damper positions will, in turn, affect the duct static pressure, creating disturbances on the fan speed control system and on variable operation conditions.

Due to its nonlinear feature, the frequently variable operation conditions and external disturbances, coupled with system interactions, make the fan control system design and operation a significant challenge (Mei and Levermore 2000). To achieve good operation performance in addition to low energy cost, it is critical to apply more effective control strategies to the fan speed control system to handle these nonlinearities. To do so, the fan speed control system model needs to be developed and the main factors that cause the nonlinearities have to be identified.

Zaheer-Uddin and Zheng (Zaheer-Uddin and Zheng 1994) built a fan speed control system model through theoretical analysis by using nonlinear time-varying equations. However, the theoretical model is complicated, and numerous system operation parameters are required, which is generally not feasible in practice. Mei and Levermore (Mei and Levermore 2002) developed a nonlinear dynamic fan model by combining the artificial neural network (ANN)-trained fan performance curves and a first-order equation with different time constants at various operation conditions. While the model is able to reproduce the trend in fan control performance, the accuracy, especially for closed-loop control systems, is limited and large datasets have to be collected to train the model, which is costly and time consuming. Similarly, Raisoni, Raman et al. (Raisoni, Raman et al. 2018) developed a low order control-oriented model to predict the fan airflow rate in response to changes in fan speed and damper positions by introducing the dynamics into the steady-state functions. The control-oriented model is aimed at real-time control computations. While the model can be used for control system design, a variety of tests

have to be conducted to calibrate the unknown parameters. Wang and Wang (Wang and Wang 2008) pointed out the difficulty in establishing the theoretical fan speed control system model. They obtained the relationship among the fan speed, airflow rate and duct static pressure through experimental methods by measuring the duct static pressure variation as the fan airflow rate is changed under different fan speeds while the time constant of the system response is neglected. In conclusion, the fan speed control system models built above are computationally complicated and time-consuming. In addition, none of the studies have explicitly pointed out the component gain variations under various operation conditions, and the key factors that impact the system nonlinear control performance still remain unknown.

On the other hand, the controller designed for a traditional fan speed control system is a Proportional-Integral-Derivative (PID) controller with fixed gains. With such a controller, the nonlinear system can become sluggish or oscillatory when its operation condition deviates significantly from the condition where the controller is tuned (Singhal and Salsbury 2007). Specifically, the system can experience instability when it operates at low load conditions if the controller is tuned at high load conditions, while the system can behave sluggishly at high load conditions if the controller is tuned at low load conditions (Underwood 2002, Moradi, Saffar-Avval et al. 2011, Price and Rasmussen 2015). Mei and Levermore (Mei and Levermore 2000) investigated the range of stability for the gains of the Proportional-Integral (PI) controller of a nonlinear fan speed control system with all the component gains and time constants fixed under various operation conditions. The experiments showed that the gains of the PI controller have a larger stable range with a higher airflow rate, indicating that the system

nonlinear control performance can be impacted by the airflow rate, and the system can become unstable with a low airflow rate with a fixed duct static pressure. In fact, undesired oscillations have often been observed in fan speed control systems. Tests conducted on ten AHUs resulted in oscillations in 22% of the supply fans for 6% – 26% of their operating time (Chintala, Price et al. 2015). While the oscillations can result in higher supply fan energy consumption, thermal comfort complaint and device wear, more effective and practical control strategies are desired to handle the control issues caused by the system nonlinearities.

Optimal, predictive, and adaptive controllers have been studied extensively to resolve the nonlinearities of the control systems. However, while these controllers are considered cutting-edge, the applications of them in practice in the replacement of PID controllers are impeded by their intensive computation and complex control algorithm (Okochi and Yao 2016). Therefore, this paper aims at developing an efficient yet effective control algorithm for fan speed control systems.

Gain scheduling control, as one type of adaptive control strategy, is a popular solution to nonlinear control design problems with a large range of operation condition variations and system nonlinearities for its inherited benefits of PID controller with intuitive design. Classical gain scheduling control depends on the dynamic characteristics of a nonlinear system, which can be described as a combination of a family of linear time invariant (LTI) systems and the local controllers tuned based on the LTI system under the current operation conditions. Shin, Chang et al and Moradi, Saffar-Avval et al (Shin, Chang et al. 2002, Moradi, Saffar-Avval et al. 2011) both applied the classical gain scheduling control strategy to the control system in an AHU and achieved better control performance and less energy

consumption. Wu, Li et al (Wu, Li et al. 2019) designed a gain scheduling controller based on active disturbance rejection control for thermal power plant under full operation conditions. However, there are some drawbacks of classical gain scheduling control. It requires accurate LTI models for linear controller design, which may be difficult or even infeasible to obtain for some systems. On the other hand, it may result in unsatisfactory or even unstable control performance for systems with rapid parameters change. To handle the limitations of classical gain scheduling control, gain scheduling synthesizing adaptive fuzzy control, model predictive control (MPC) and neural network (Yang and Yan 2016, Barbosa, Bertolin et al. 2018, Ghefiri, Garrido et al. 2018, Yueneng and Ye 2018, Eltayeb, Rahmat et al. 2019, Gallego, Merello et al. 2019) has been studied to optimize the control performance and improve the robustness without the need of the LTI models. However, the gain scheduling control strategies found in literature either require multiple controllers tuning or complex control algorithm design, which can be computationally complicated and their practical application is limited (Afram and Janabi-Sharifi 2014). In addition, they can only achieve local desired performance while the global performance and stability cannot be guaranteed (Naus 2009). In contrast, the linear parameter varying (LPV) model-based gain scheduling control can avoid the model linearization and multiple controller tuning processes in addition to its prior guarantees of stability and performance specifications (Naus 2009), which has also been applied in many fields. Tahersima, Stoustrup et al. (Tahersima, Stoustrup et al. 2013) designed a gain scheduling controller based on the developed LPV model of radiator dynamics. In their study, the LPV model was developed with the radiator gain and the time constant derived as a function of the hot water flow rate and room air temperature, based on which the scheduling

function is designed to compensate the variable dynamics and transform the nonlinear system into a LTI system, which is independent of the operation conditions.

While the LPV model-based gain scheduling control shows attractive superiority, the availability of the LPV model presents the most challenges for its application. As a result, the promising gain scheduling control approach has never been studied in fan speed control systems due to the lack of simple enough LPV model. To fill the research gap, this paper aims at the development of a control-oriented model of the fan speed control systems, which can explicitly express the system nonlinearities with readily available operation parameters, paving the way for the LPV model-based gain scheduling control scheme.

Therefore, the objective of this paper is to develop and validate a gain scheduling control strategy, which can be readily implemented without additional cost, to improve the nonlinear control performance of the fan speed control system at AHUs under variable operation conditions. First, a control-oriented model of the fan speed control system is developed and calibrated, which correlates the fan system gain to the readily measurable duct static pressure and fan speed to identify the fan system nonlinearity. Then, with the developed model and experimental results, the issue of an aggressive response with a fixed-gain controller is identified under the operation conditions with a higher fan system gain, which does not meet the design conditions. Finally, a gain scheduling control strategy is developed by adding a gain scheduling function using the measurable duct static pressure and fan speed to compensate for the variable fan system gain, and the control performance improvement is validated by experiments.

2. Configuration and specifications of the test fan speed control system

Before the model development and control performance validation, the general configuration of the fan control system at a single duct AHU and the test AHU specifications are briefly introduced.

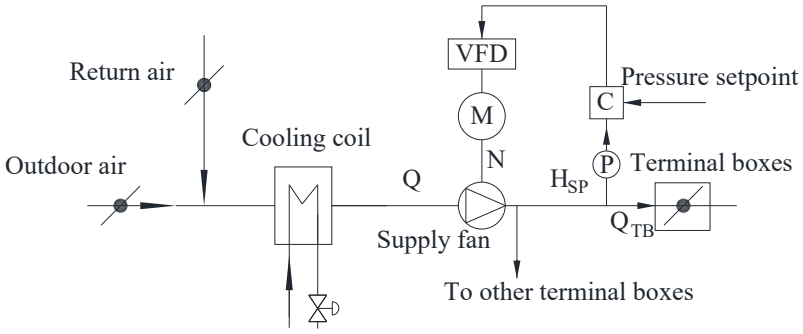

Fig. 1. Schematic of fan speed control at an AHU.

Figure 1 shows the schematic of a single duct AHU, which consists of an outdoor air section with interlinked outdoor air and return air dampers, a cooling coil, and a supply air fan. The supply fan delivers the supply air (Q) cooled by the cooling coil to TBs to achieve space thermal comfort. The damper of the pressure-independent TBs is adjusted to maintain the TB airflow rate (Q_{TB}) at its setpoint, which is determined by the space air temperature control loop associated with the space temperature setpoint and limited by the TB minimum and maximum airflow rate setpoints. Furthermore, the TB damper position will impact the duct static pressure (H_{sp}) measured by a pressure differential sensor (P), which is the duct static pressure referring the conditioned space. Therefore, the pressure loss on ducts downstream from the pressure differential sensor equals the value measured by the pressure differential sensor plus the space static pressure. Ideally, the space positive static pressure recommended by ASHRAE is 1 Pa (0.004 inch of water) (ASHRAE 2007), which is small and can be ignored. In this case, the duct static pressure reflects the pressure loss of the downstream ducts. Meanwhile, the supply

fan that is driven by a motor (M) creates the fan head to overcome the pressure losses through the air distribution system. The fan speed (N) is modulated by a VFD to maintain the duct static pressure at its setpoint. The initial duct static pressure setpoint was 249 Pa (1.0 inch of water). However, due to energy efficient lighting and office equipment upgrade in spaces, the space cooling load and associated supply airflow rate were significantly less than the initial design values. A new duct static pressure was identified as 124 Pa (0.5 inch of water), which can ensure that all the TBs can receive the required airflow at actual operation conditions in the afternoon during the hot summer.

To calibrate the developed model and validate the control performance improvement using the gain scheduling control strategy, tests were conducted on a single duct AHU that serves an education building in Norman, Oklahoma. The duct static pressure differential sensor is located two-thirds of the way downstream of the supply air duct with four TBs at its downstream and three TBs at its upstream. The fan is driven by a 3ph 208V 3HP motor, with a design fan airflow rate of 1180 L/s (2,500 CFM) and a design fan head of 547 Pa (2.2 inch of water).

The fan speed was initially controlled by a well-tuned fixed-gain PI controller with a P gain of 0.44%/Pa (110%/inch of water) and an I gain of 0.044%/Pa-second (11%/inch of water-second) to achieve the desired control performance with 20% overshoot under the operation condition where the duct static pressure setpoint is 124 Pa (0.5 inch of water) and the fan speed is 55Hz. The transfer function of the PI controller with the fixed gains is expressed as:

$$C_{fix} = P + \frac{I}{s} \tag{1}$$

During the tests, the VFD frequency command and fan speed (VFD output frequency feedback) were directly obtained from the VFD. The fan airflow rate was measured using an existing air flow meter. The duct static pressure was measured using a duct static pressure differential sensor with an accuracy of ±0.4% of full scale, which is 1244 Pa (5 inch of water). All the test data were recorded at 1 second intervals.

3. Control-oriented model of fan speed control systems

In this section, the theoretical fan speed control model is first developed to identify the nonlinearity of the fan system gain. Then, the model is calibrated through three open-loop tests.

3.1 Theoretical model development

The block diagram of the fan speed control system defined in Figure 1 with the reference input and the disturbance input is shown as Figure 2. The controlled variable (C) is the supply air duct static pressure; the reference input (R) is the setpoint of the duct static pressure; the disturbance input (D) is the TB airflow setpoint change, which will lead to the TB damper position change and consequently disturb the duct static pressure. There are three components of the fan speed control system model, in addition to the controller: the VFD-motor, the fan-duct, and the duct static pressure differential sensor.

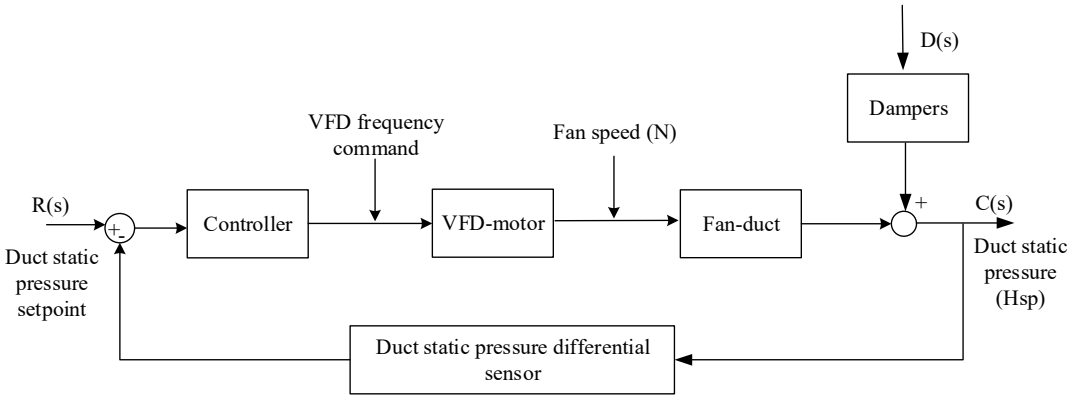

Fig. 2. Block diagram of traditional single-loop fan speed control.

(1) Fan-duct model

The transfer function of the fan-duct component can be modeled as a first-order system at each operation condition.

$$G_{fd} = \frac{K_{fd}}{\tau_{fd}s+1} \tag{2}$$

where K_{fd} is the fan-duct gain, defined as the ratio of the duct static pressure change to the fan speed change, and τ_{fd} is the fan-duct time constant at each operation condition.

Theoretically, the fan-duct transfer function is derived from its dynamic physical model by linearizing the nonlinear differential equation using the Taylor series expansion (Nise 2019). Considering the complexity, the nonlinear dynamic fan system can be analyzed by a Hammerstein model, which consists of a model of a nonlinear static system and a model of a linear dynamic system (Lennart 1999). To develop the fan-duct model, the nonlinear steady-state (static) model can be developed first, and the dynamics can be introduced by adding in the time constant at each operation condition, which follows the same procedure in previous studies (Mei and Levermore 2002, Raisoni, Raman et al. 2018).

Since the pressure loss of the ducts (DP) downstream from the pressure differential sensor is proportional to the supply airflow rate squared (Shim, Song et al. 2014), the duct static pressure (H_{sp}) plus the space static pressure (H_{space}) is determined by the airflow rate through the downstream TBs and the resistance coefficient of the downstream ducts and TBs.

$$DP = H_{sp} + H_{space} = S_{TB}(Q_{TB})^2 = S_{TB}(\alpha Q)^2 \tag{3}$$

where α is the ratio of the airflow rate through the TBs (Q_{TB}) downstream from the duct static pressure differential sensor to the fan airflow rate (Q); S_{TB} is the lumped resistance coefficient of the downstream ducts and TBs of the duct static pressure differential sensor, which is determined by the TB damper positions. The TB damper positions can be considered static within a very short time period when the fan speed experiences a small excursion. In this case, the lumped resistance coefficient (S_{TB}) can be considered constant.

According to the affinity laws, with fixed damper positions (i.e., the same resistance coefficient), the fan airflow rate (Q) is proportional to the fan speed (N).

$$Q = \beta N \tag{4}$$

where β is the constant ratio of the fan airflow rate to the fan speed at fixed TB damper positions. By combining Eq. (3) and Eq. (4), the nonlinear relationship between the pressure loss on ducts downstream from the pressure differential sensor, which equals the duct static pressure (H_{sp}) plus the space static pressure (H_{space}), and the fan speed (N), is obtained as Eq. (5).

$$DP = H_{sp} + H_{space} = S_{TB}(\alpha\beta)^2 N^2 \tag{5}$$

Therefore, by conducting the Taylor series expansion, the duct pressure loss change, which is also the duct static pressure change if the space static pressure remains constant, can be expressed by Eq. (6):

$$\Delta H_{sp} = \Delta DP = \frac{\partial H_{sp}}{\partial N}\Delta N + \frac{\partial^2 H_{sp}}{\partial N^2}\frac{(\Delta N)^2}{2} = 2S_{TB}(\alpha\beta)^2 N \cdot \Delta N + S_{TB}(\alpha\beta)^2(\Delta N)^2 \tag{6}$$

Thus, the fan-duct gain (K_{fd}), the ratio of the duct static pressure change to the fan speed change, can be calculated with the duct static pressure (H_{sp}) and the fan speed (N) at each steady-state operation condition, shown as Eq. (7).

$$K_{fd} = \frac{\Delta H_{sp}}{\Delta N} = 2\frac{(H_{sp}+H_{space})}{N} + \frac{\Delta N}{N^2}(H_{sp} + H_{space}) \quad (7)$$

For small space static pressure ($H_{space} \approx 0$) and small excursion of the fan speed ($\Delta N \approx 0$), the fan-duct gain is ideally proportional to the ratio of the duct static pressure (H_{sp}) to the fan speed (N) at each operation condition, which indicates the nonlinearity of the fan-duct component as well as the fan speed control system.

$$K_{fd} = 2\frac{H_{sp}}{N} \quad (8)$$

Then, for the dynamic model, the dynamics can be introduced to the steady-state fan-duct gain in Eq. (8) with the fan-duct time constant (τ_{fd}) calibrated through step change response tests.

(2) VFD-motor model

Because of the ramping feature of VFDs (Hao, Lin et al. 2014) and the linear relationship between the VFD frequency command and fan speed (Joo, Liu et al. 2007), the transfer function of the VFD-motor component (G_{Vm}) can be modeled as a first-order system.

$$G_{Vm} = \frac{K_{Vm}}{\tau_{Vm}s+1} \quad (9)$$

where K_{Vm} is the VFD-motor gain, defined as the ratio of the fan speed change to the VFD frequency command change, and τ_{Vm} is the VFD-motor time constant.

(3) Duct static pressure differential sensor

In practice, the duct static pressure differential sensor can also be modeled as a first-order system. The sensor gain is one if the duct static pressure setpoint has the same unit as the measured duct static pressure. The time constant's value is constant and available from the sensor manufacturer.

$$G_s = \frac{1}{\tau_s s+1} \tag{10}$$

Therefore, the system model (G_{sys}) at a particular operation condition, including the fan-duct model (G_{fd}), VFD-motor model (G_{Vm}), and duct static pressure differential sensor (G_s) can be expressed as Eq. (11) .

$$G_{sys} = \frac{K_{sys}}{(\tau_{Vm}s+1)(\tau_{fd}s+1)(\tau_s s+1)} = \frac{K_{Vm}\cdot 2\frac{H_{sp}}{N}}{(\tau_{Vm}s+1)(\tau_{fd}s+1)(\tau_s s+1)} \tag{11}$$

where K_{sys} refers to the system gain, i.e., the product of the VFD-motor gain and the fan-duct gain.

3.2 Model calibration through open-loop tests

To calibrate the system model, an open-loop test was conducted by fixing the TB damper at different positions and incrementally changing the fan speed from 29Hz to 38Hz, 47Hz, 56Hz and 58Hz with a step change of the VFD frequency command. Since the control system uses two digital signals, either an opening or closing command, to control the TBs without the damper position information, the TB damper position can only be accurately controlled to be fully open or closed. To fully open one TB, the minimum airflow setpoint was set to be higher than its capacity. To fully close one TB, on the other hand, the maximum airflow setpoint was set to be zero. During the tests, the number of fully closed TBs was controlled to generate different operation conditions. For example, increasing the number of fully closed TBs is equivalent to reducing the wide-open position of the TB dampers. All the TBs were fully open in the first test, and two TBs at the downstream and one TB at the upstream were fully closed in

the second test. Finally, three TBs at the downstream and two TBs at the upstream were fully closed in the third test.

The duct static pressure differential sensor had a time constant (τ_s) of 0.25 seconds according to the manufacturer, while its gain was 1 Pa/Pa (1.0 inch of water/inch of water). The first-order transfer functions of the VFD-motor and fan-duct are obtained from the open-loop step response tests by measuring the steady-state value and the time constant, which is the time for the amplitude to reach 63% of its final value, at each operation condition (Nise 2019). The transfer function of the VFD-motor component (G_{Vm}) was identified with the gain (K_{Vm}) equal to 0.6 Hz/% and the time constant (τ_{Vm}) equal to 3 seconds regardless of operation conditions. In addition, the fan-duct time constant (τ_{fd}) was approximated as 0.5 seconds, which was also independent of the operation condition. On the other hand, the fan-duct gain was measured to be varied under various operation conditions. Table 1 shows the fan-duct gain (K_{fd}) and the ratio of the duct static pressure (H_{sp}) to the fan speed (N) under various operation conditions of the three open-loop tests.

Table 1: Fan-duct gain and $\frac{H_{sp}}{N}$ under various operation conditions.

Test	Fan airflow rate L/s (CFM)	Duct static pressure Pa (inch of water)	Fan speed (Hz)	$\frac{H_{sp}}{N}$ Pa/Hz (inch of water/Hz)	Theoretical fan-duct gain Pa/Hz (inch of water/Hz)	Experimental fan-duct gain Pa/Hz (inch of water/Hz)
All TBs open	474 (1,004)	-7.5 (-0.03)	29	-0.25 (-0.0010)	-0.50 (-0.0020)	4.4 (0.018)
	633 (1,341)	32 (0.13)	38	0.82 (0.0033)	1.6 (0.0066)	5.7 (0.023)
	787 (1,667)	85 (0.34)	47	1.7 (0.0070)	3.5 (0.014)	7.9 (0.032)
	906 (1,919)	152 (0.61)	56	2.7 (0.011)	5.4 (0.022)	8.5 (0.034)

Three TBs closed	416 (881)	17 (0.07)	29	0.47 (0.0019)	0.95 (0.0038)	6.6 (0.026)
	550 (1,165)	75 (0.30)	38	1.9 (0.0075)	3.7 (0.015)	8.6 (0.035)
	666 (1,412)	152 (0.61)	47	3.2 (0.013)	6.3 (0.025)	11 (0.043)
Five TBs closed	293 (621)	70 (0.28)	29	2.1 (0.0084)	4.2 (0.017)	9.3 (0.038)
	372 (788)	147 (0.59)	38	3.7 (0.015)	7.5 (0.030)	12 (0.048)
	442 (936)	259 (1.04)	47	5.3 (0.021)	11 (0.0428)	14 (0.058)
	480 (1,018)	376 (1.51)	56	6.7 (0.027)	13 (0.054)	17 (0.068)

Figure 3 compares the experimental and ideal theoretical fan-duct gain versus the ratio of the duct static pressure to the fan speed. The red circle marker represents the experimental fan-duct gain measured through the tests while the black line represents the ideal theoretical relationship between the fan-duct gain and the ratio of the duct static pressure to the fan speed based on Eq. (8).

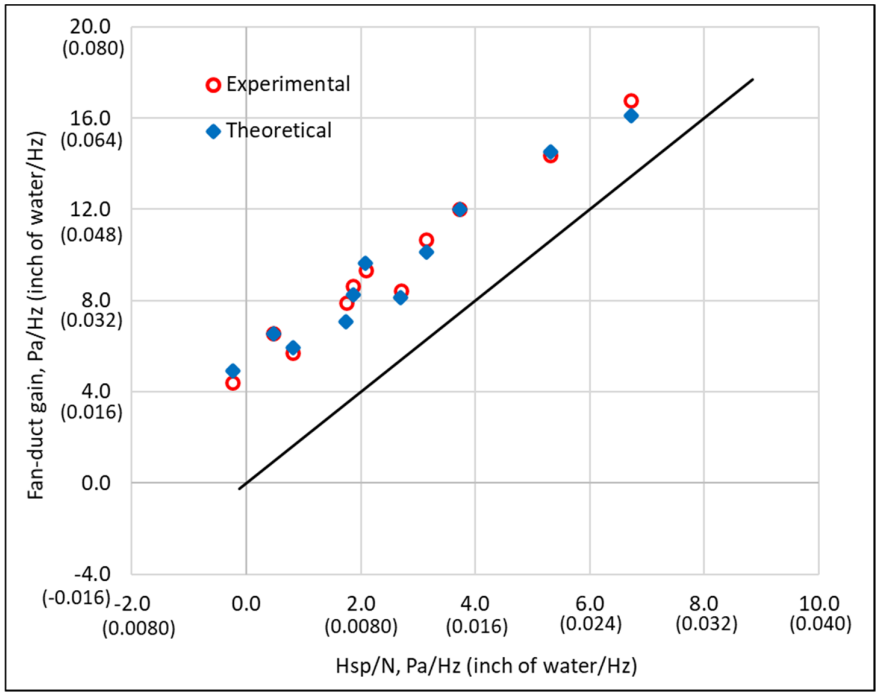

Fig. 3. $\frac{H_{sp}}{N}$ vs. fan-duct gain.

It reveals that the experimental fan-duct gain is larger than the ideal theoretical fan-duct gain. As previously stated, the ideal theoretical fan-duct gain is derived based on three assumptions, (1) the fan airflow rate conforms the affinity laws, defined by Eq. (4); (2) the duct static pressure conforms the affinity laws with the small space static pressure ($H_{space} \approx 0$), defined by Eq. (5); (3) the fan speed excursion is small ($\Delta N \approx 0$).

As for the first assumption, Figure 4 presents the fan airflow rate versus the fan speed with the TBs fully open as an example, which proves that the fan airflow rate is proportional to the fan speed and the affinity laws can be applied as in Eq. (4).

As for the second assumption, Table 1 shows a negative duct static pressure when the fan speed is 29Hz with all the TBs fully open, which indicates that the space positive static pressure may be considerably too large to be neglected. Furthermore, Figure 5 shows the duct static pressure versus the fan speed (cross marker) measured by the pressure differential sensor. The measured correlation does not conform to the affinity laws defined by Eq. (5) and the space static pressure was not small. Then the space static pressure was identified to be 62 Pa (0.25 inch of water) to ensure that the duct pressure loss, the sum of the duct static pressure and the space static pressure, is proportional to the fan speed squared, which is represented by triangle markers in Figure 5.

As for the third assumption, the fan speed excursion reaches around 9Hz, which is not small enough, and the third assumption also needs to be reconsidered.

Therefore, by considering the considerable space static pressure and fan speed change, the theoretical fan-duct gain is recalculated using Eq. (7) and shown in Figure 3 with the blue diamond marker, which matches well with the experimental fan-duct gain. This means that the experimental fan-duct gain can match with the theoretical value and the fan-duct gain model defined by Eq. (7) is validated.

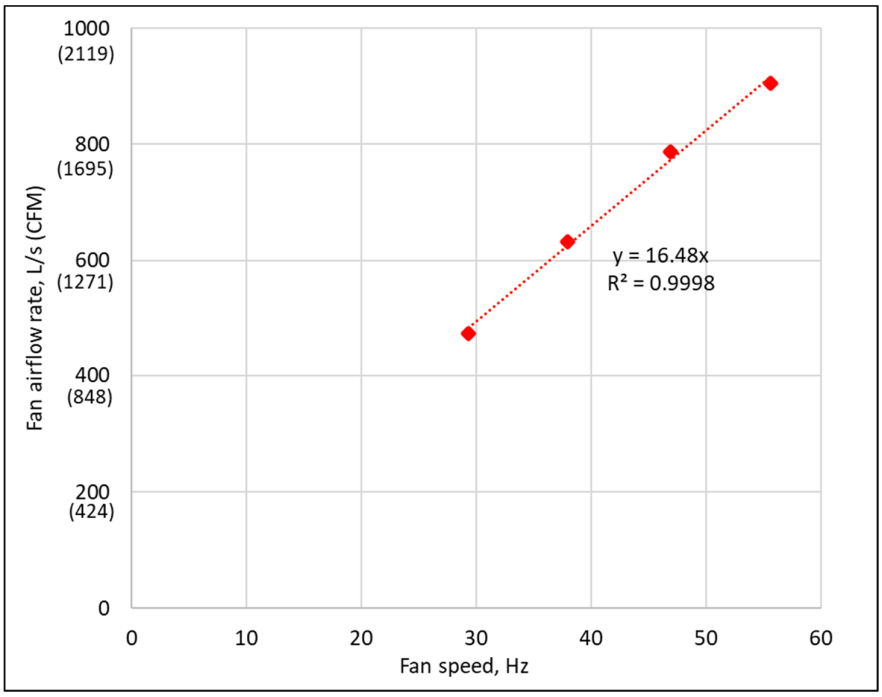

Fig. 4. Fan speed vs. fan airflow rate.

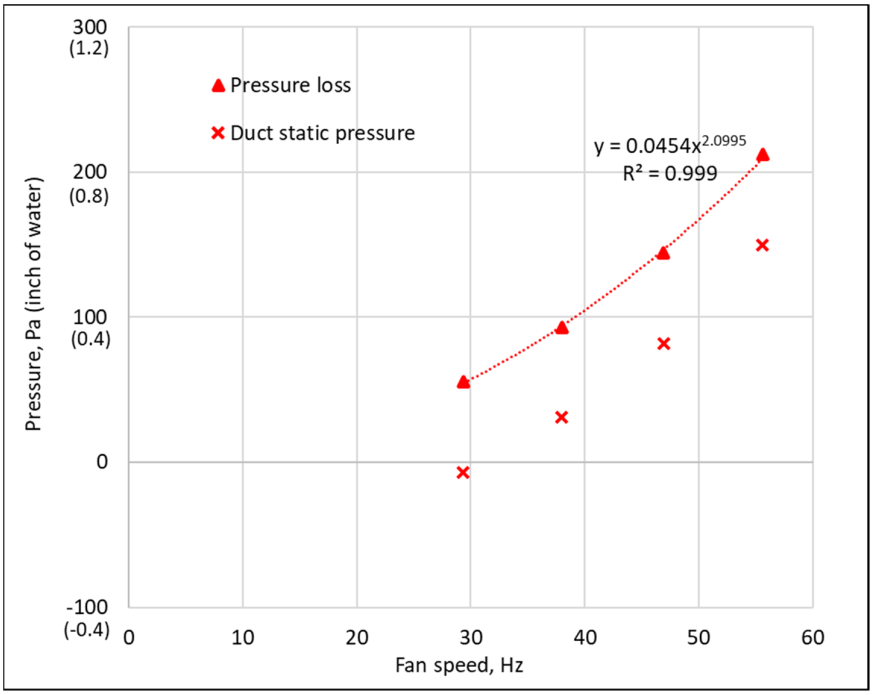

Fig. 5. Fan speed vs. pressure loss of the downstream ducts.

To conclude, the time constants of all the components and the gains of all components except the fan-duct component can be considered constant. Under a normal operation where the space static pressure and fan speed change are small, the fan-duct gain (K_{fd}) is proportional to the ratio of the duct static pressure to the fan speed, which is supposed to be the main factor that causes the nonlinearities of the fan speed control system.

4. Control performance validation with a fixed-gain controller

According to the developed fan speed control model, with a fixed-gain controller, the system will have a larger system gain and consequently more aggressive response under the operation conditions with lower fan speed or higher duct static pressure, i.e., a larger ratio of the duct static pressure to the fan speed.

4.1 Tests with variable fan speed and constant duct static pressure

To validate the control performance impacted by the variable fan speed, the TB damper position was overridden with different numbers of fully closed TBs to create various partial load conditions, while the duct static pressure setpoint was fixed at 124 Pa (0.5 inch of water). At each operation condition, the system was maintained for more than 17 minutes. In Test condition 1, two TBs were set to be fully closed. Then the two fully closed TBs were set to be fully open in Test condition 2. Afterward, one TB plus two TBs closed in Test condition 1 were set to be fully closed in Test condition 3. Meanwhile, the remaining TBs maintained their original airflow setpoints.

Figure 6 presents the system response of the fan speed (blue line) and duct static pressure (red line). The fan speed varies from 39Hz to 43Hz and 37Hz while the duct static pressure oscillates around its setpoint of 124 Pa (0.5 inch of water). Figure 7 presents the fan airflow rate (yellow line) and the ratio of the duct static pressure to the fan speed (green line) with variable fan speed. The corresponding fan airflow rate varies from 475 L/s (1,007 CFM) to 566 L/s (1,199 CFM) and 400 L/s (848 CFM).

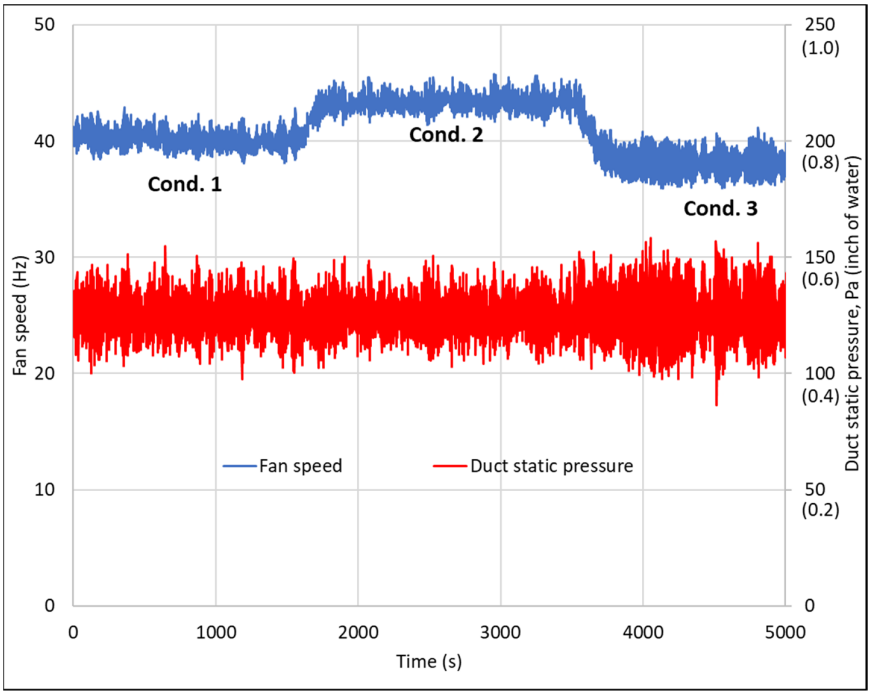

Fig. 6. System response of fan speed and duct static pressure with variable fan speed.

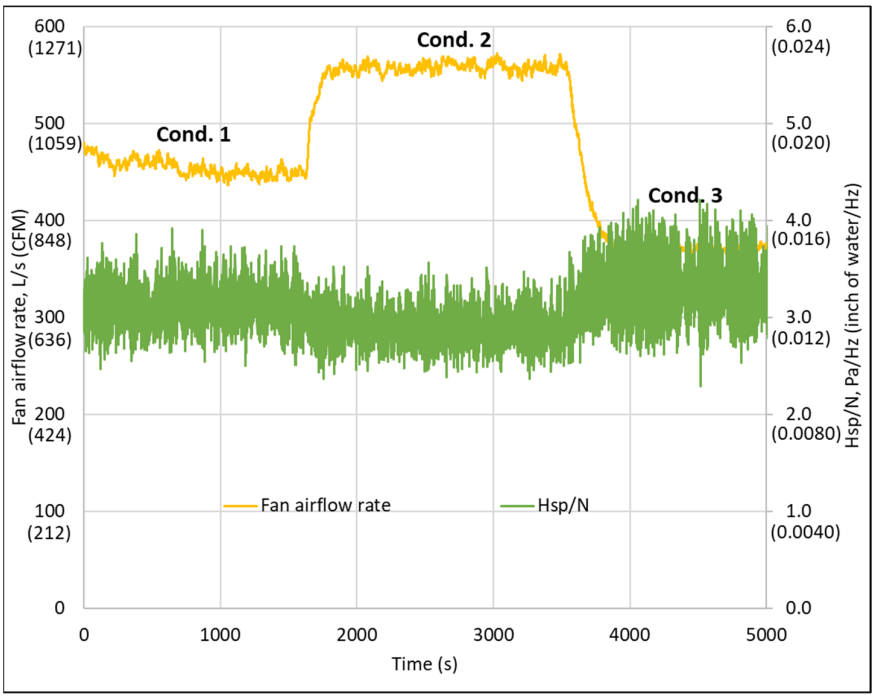

Fig. 7. Fan airflow rate and $\frac{H_{sp}}{N}$ with variable fan speed.

4.2 Tests with variable fan speed and variable duct static pressure

To validate the control performance impacted by the variable duct static pressure in addition to the fan speed, the duct static pressure setpoint was incrementally changed from 100 Pa (0.4 inch of water) in Test condition 4 to 149 Pa (0.6 inch of water) in Test condition 5, 199 Pa (0.8 inch of water) in Test condition 6 and 249 Pa (1.0 inch of water) in Test condition 7 while the TB airflow setpoint was fixed by setting all the TBs' maximum and minimum settings as fixed values. Similarly, at each operation condition, the system was maintained for more than 17 minutes.

As discussed previously, the optimal duct static pressure is 124 Pa (0.5 inch of water) for the actual operation conditions and the goal of using the duct static pressure setpoints higher than the optimal setpoint is to validate the control performance impacted by the variable duct static pressure and the improvement by using the gain scheduling controller.

Figure 8 presents the system response of the fan speed (blue line) and duct static pressure (red line), while Figure 9 presents the fan airflow rate (yellow line) and the ratio of the duct static pressure to fan speed (green line) with duct static pressure change. It can be observed that the fan airflow rate remains almost constant.

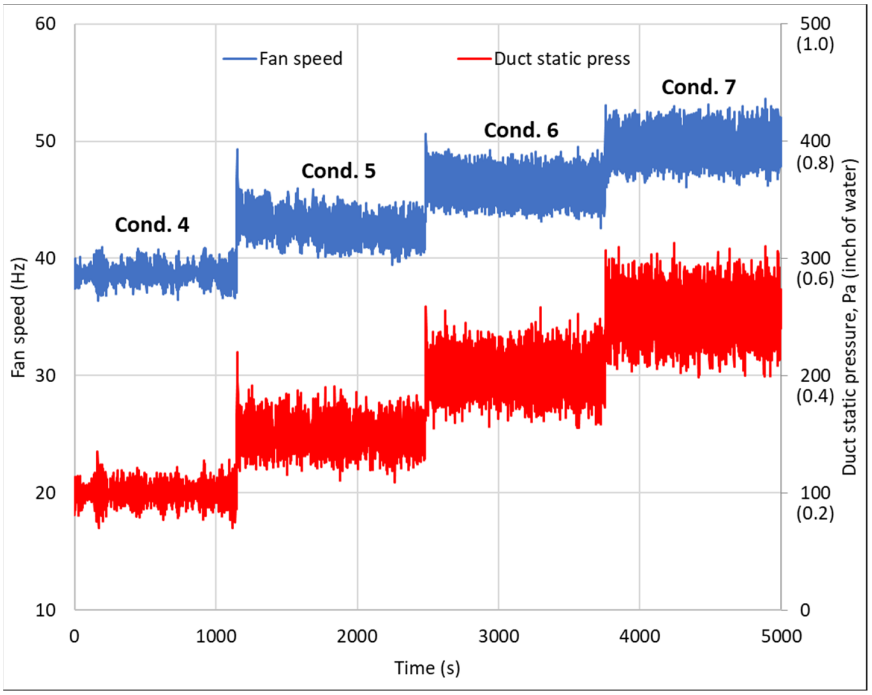

Fig. 8. System response of fan speed and duct static pressure with variable duct static pressure.

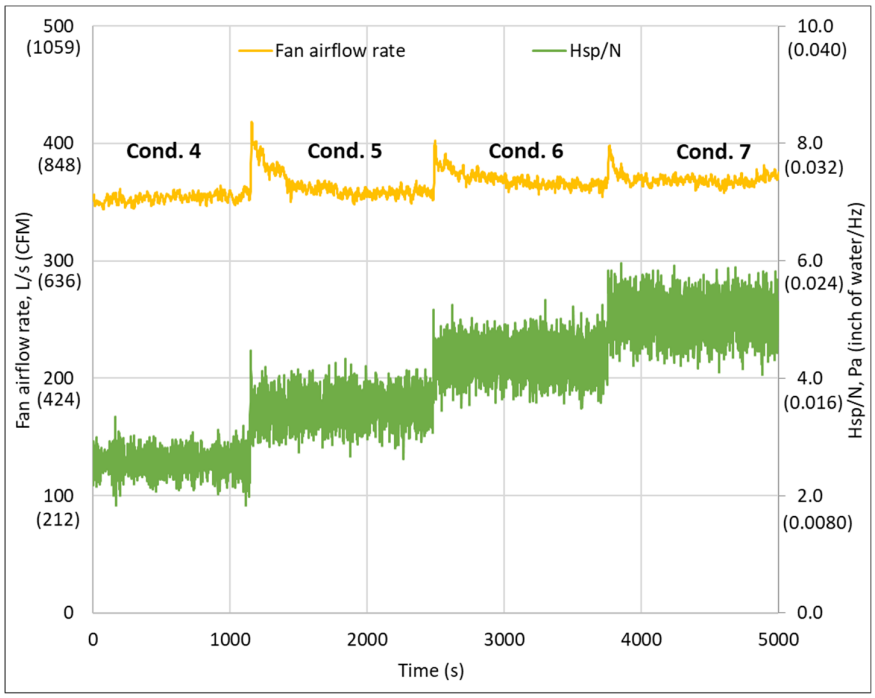

Fig. 9. Fan airflow rate and $\frac{H_{sp}}{N}$ with variable duct static pressure.

Table 2 lists the fan airflow rate, duct static pressure, fan speed and the corresponding ratio of the duct static pressure to the fan speed under the seven test conditions.

Table 2: Test conditions.

Test condition	Fan airflow rate L/s (CFM)	Duct static pressure Pa (inch of water)	Fan speed (Hz)	$\frac{H_{sp}}{N}$ Pa/Hz (inch of water/Hz)
Cond. 1	475 (1,007)	124 (0.5)	39	3.2 (0.013)
Cond. 2	566 (1,199)	124 (0.5)	43	3.0 (0.012)
Cond. 3	400 (848)	124 (0.5)	37	3.5 (0.014)
Cond. 4	385 (817)	100 (0.4)	39	2.5 (0.010)
Cond. 5	364 (772)	149 (0.6)	43	3.5 (0.014)
Cond. 6	364 (771)	199 (0.8)	46	4.2 (0.017)
Cond. 7	368 (779)	249 (1.0)	50	5.0 (0.020)

4.3 Control performance evaluation with a fixed-gain controller

Specifically, to comprehensively evaluate the performance of the fan speed control system, the quantitative specifications, such as the rise time, settling time and overshoot, are expected to be computed. However, the system response is too fast to accurately catch the dynamic response specifications using the recorded data with a sampling time of 1 second.

Therefore, the control performance impacted by the noise and system oscillation at the steady-state conditions was evaluated by using three indices, including the oscillation range of the fan speed and duct static pressure, and the root mean squared error (RMSE) of the duct static pressure.

The oscillation range was defined as the difference between the average maximum value and the average minimum value of the fan speed or duct static pressure at each operation condition; the RMSE

of the duct static pressure was calculated using Eq. (12). Since the fan speed varies as the operation condition is changed, the RMSE of the fan speed was not evaluated.

$$RMSE = \sqrt{\frac{\sum_{j=1}^{n}(H_{spj,measured} - H_{spj,setpoint})^2}{n}} \quad (12)$$

where $H_{spj,measured}$ and $H_{spj,setpoint}$ refer to the measured value and the setpoint of the duct static pressure at the jth sample respectively; n is the total number of the measured samples. Table 3 lists the oscillation range of the fan speed and duct static pressure as well as the RMSE of the duct static pressure under the seven test conditions.

Table 3: Oscillation range and RMSE under the seven test conditions.

Test condition	Fan speed oscillation range (Hz)		Duct static pressure oscillation range Pa (inch of water)		RMSE of duct static pressure Pa (inch of water)	
	Fixed	Gainsched	Fixed	Gainsched	Fixed	Gainsched
Cond. 1	1.8	0.9	22 (0.088)	14 (0.055)	8.7 (0.035)	5.7 (0.023)
Cond. 2	**1.6**	**1.0**	**19 (0.075)**	**15 (0.059)**	**7.7 (0.031)**	**6.0 (0.024)**
Cond. 3	2.8	0.8	32 (0.13)	12 (0.050)	12 (0.048)	5.7 (0.023)
Cond. 4	1.8	1.4	20 (0.081)	19 (0.076)	8.5 (0.034)	7.7 (0.031)
Cond. 5	3.4	1.2	42 (0.17)	20 (0.079)	15 (0.062)	8.2 (0.033)
Cond. 6	4.1	1.0	52 (0.21)	22 (0.084)	20 (0.081)	9.7 (0.039)
Cond. 7	**4.7**	**0.9**	**69 (0.28)**	**25 (0.10)**	**24 (0.098)**	**10 (0.043)**

By comparing the performance among Test conditions 1-3, it can be observed that, with fixed duct static pressure, the system response becomes more aggressive under lower fan speed and lower airflow rate with larger values of the three indices. Similarly, by comparing the performance among Test conditions 4-7, the system has more aggressive response with larger values of the three indices under higher duct static pressure. On the other hand, the duct static pressure reset, which reduces the duct static pressure setpoint to achieve lower fan speed at partial load conditions, will have a sluggish

response. Meanwhile, the TBs with airflow control tend to maintain the same fan airflow after the transient period while the control performance is significantly different, indicating that the fan airflow rate is not a factor that impacts the system performance.

Specifically, with the fixed-gain controller, the system has the worst control performance under Test condition 7 with fan speed at 50Hz and duct static pressure at 249 Pa (1.0 inch of water), where the ratio of the duct static pressure to fan speed also has the largest value of 5.0 Pa/Hz (0.02 inch of water /Hz). In this case, the oscillation range of the fan speed reaches up to 4.7Hz, while the oscillation range of the duct static pressure reaches up to 69 Pa (0.28 inch of water). The RMSE of the duct static pressure reaches up to 24 Pa (0.098 inch of water). Compared to the performance at Test condition 2 where the ratio of the duct static pressure to the fan speed is 3.2 Pa/Hz (0.013 inch of water /Hz), the oscillation ranges of the fan speed and duct static pressure as well as the RMSE of the duct static pressure are approximately tripled.

To conclude, the test results with a fixed-gain controller match the control performance indicated by the developed fan speed control model. Furthermore, the fan airflow rate alone is not sufficient enough to indicate the system nonlinearities, while the ratio of the duct static pressure setpoint to fan speed is supposed to be the better indicator.

5. Performance improvement through gain scheduling control

In this section, the gain scheduling controller is first designed. Then, the control performance improvement by implementing the designed gain scheduling controller is validated through experiments at the test conditions identical to those using the fixed-gain controller, listed in Table 2.

5.1 Gain scheduling controller design

Based on the developed fan speed control model and the validated control performance with a fixed-gain controller, the main nonlinearities of the fan speed control systems are caused by the variation of the fan-duct gain (K_{fd}), which consequently results in the variable system gain (K_{sys}), under variable operation conditions. Therefore, to compensate for its nonlinearities and achieve identical control performance under variable operation conditions, the main idea is to cancel out the variation of the system gain (K_{sys}). Specifically, its control performance can be impacted by the variable fan speed and duct static pressure while the ratio of the duct static pressure to the fan speed is more sufficient to indicate the nonlinearities under normal operation condition where the space static pressure and the fan speed change are not considerable.

Even though the space static pressure was considerably large during the model calibration tests, it is not controlled by the test AHU and is supposed to be approximately zero under the common normal operation conditions. Thus, it is still rational to apply Eq. (11) to define the system model (G_{sys}). As a result, the gain scheduling controller can be designed to compensate for the gain variation by adding a scheduling function to the existing fixed-gain controller and convert it to a new controller, which can update its parameters according to the measurable duct static pressure and fan speed. The block diagram of the gain scheduling fan speed control is shown as Figure 10. The scheduling function is designed as Eq. (13).

$$g(H_{sp}, N) = \frac{H_{sp,r}}{H_{sp}} \cdot \frac{N}{N_r} \tag{13}$$

where $H_{sp,r}$ and N_r are the duct static pressure and fan speed under a reference condition, where the fixed gain controller results in a desired control performance of the AHU fan. For the test system, the reference fan speed is 55Hz and the reference duct static pressure is 124 Pa (0.5 inch of water). Consequently, the equivalent system gain of the transformed system would be fixed at the design condition and the system is expected to have identical control behaviors under variable operation conditions.

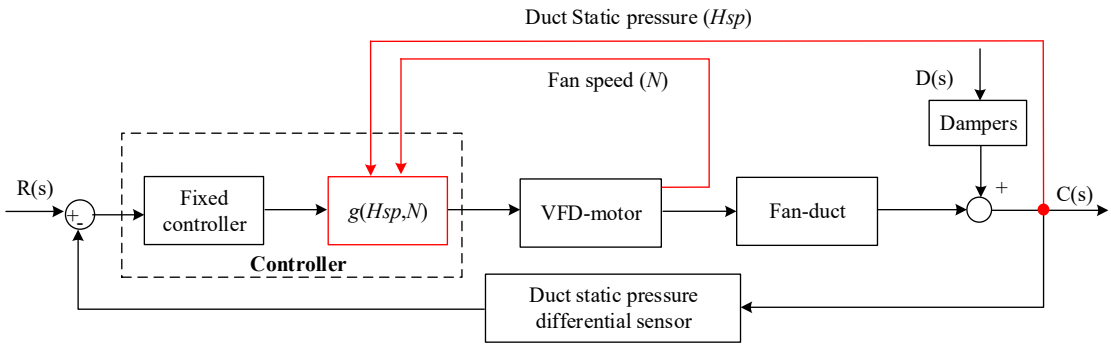

Fig. 10. Block diagram of gain scheduling fan speed control.

5.2 Gain scheduling control implementation and control performance evaluation

To validate the control performance improvement of the gain scheduling control strategy, the closed-loop tests were conducted under the seven same test conditions on the same test AHU using the gain scheduling controller designed above. For implementation, the duct static pressure setpoint rather than the measured value was applied to update the controller to avoid the measurement noise caused by the duct static pressure differential sensor.

Figure 11 compares the system response of the fan speed (a) and the duct static pressure (b) with variable fan speed under Test conditions 1 to 3 using the fixed-gain controller and gain scheduling controller, while Figure 12 compares the system response of the fan speed (a) and duct static pressure

(b) with variable duct static pressure under Test conditions 4 to 7 using the fixed-gain controller and gain scheduling controller. The blue line and the yellow line represent the fan speed using the fixed-gain controller and gain scheduling controller, respectively. The red line and the grey line represent the duct static pressure using the fixed-gain controller and gain scheduling controller, respectively. According to Eq. (13), the gain scheduling function is reversely proportional to the ratio of the duct static pressure to the fan speed, which is presented in Figure 7 and Figure 9 under all seven test conditions.

Overall, it can be observed that the system response with the gain scheduling controller has much better control performance than that with the fixed-gain controller. As the ratio of the duct static pressure to the fan speed, i.e., the fan-duct gain, increases in Test condition 3 presented in Fig.7, and increases from Test conditions 4 to 7 presented in Figure 9, the oscillation range of the fixed-gain controller increases as the fan-duct gain increases. On the other hand, as the gain scheduling function is reversely proportional to the fan-duct gain, the gain scheduling controller can effectively compensate of the fan-duct gain variation and can approximately maintain the identical control behaviors under all various operation conditions.

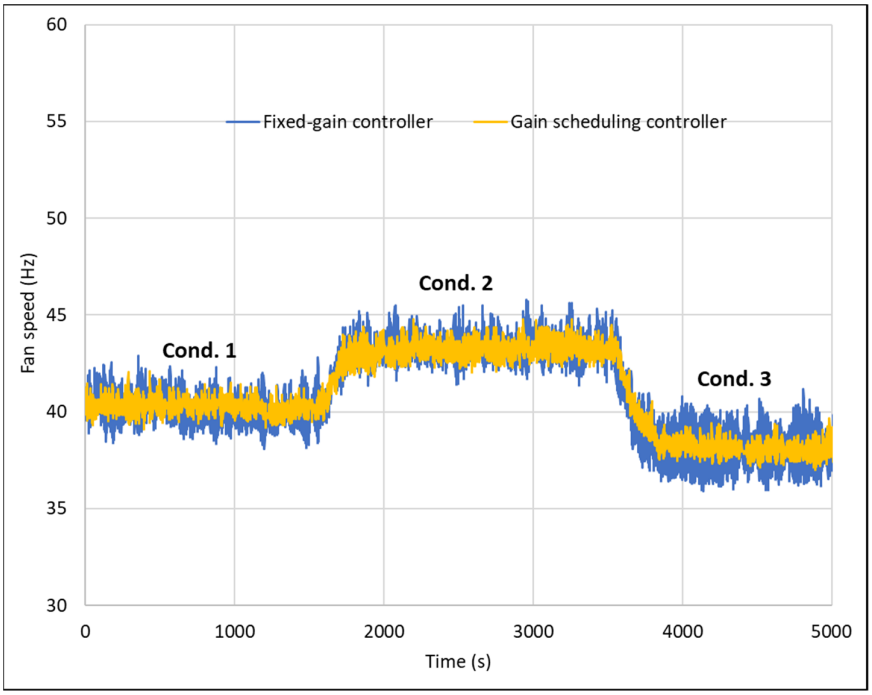

(a) System response of fan speed.

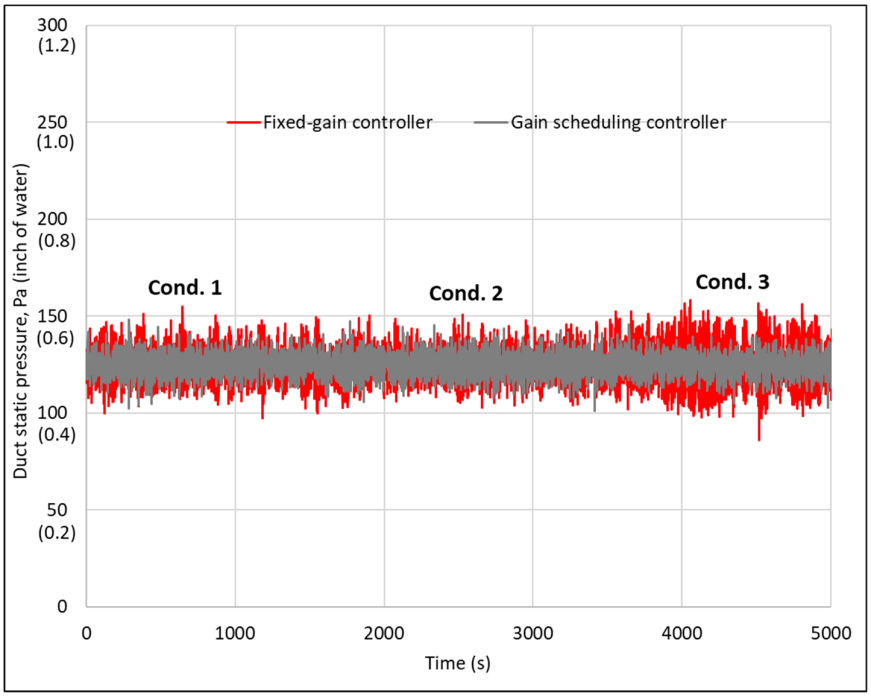

(b) System response of duct static pressure.

Fig. 11. System response with variable fan speed using the fixed-gain controller and gain scheduling controller.

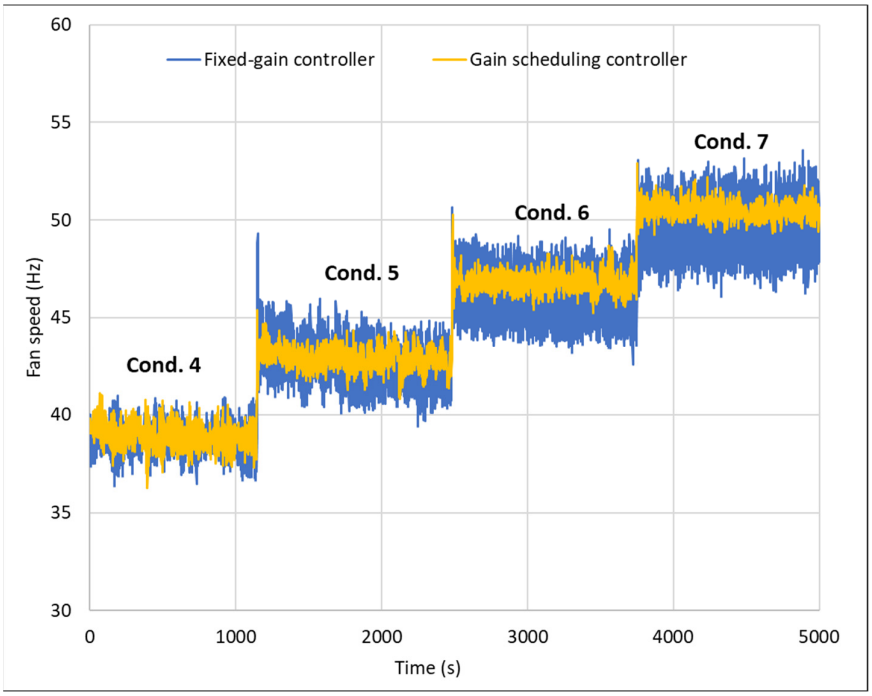

(a) System response of fan speed.

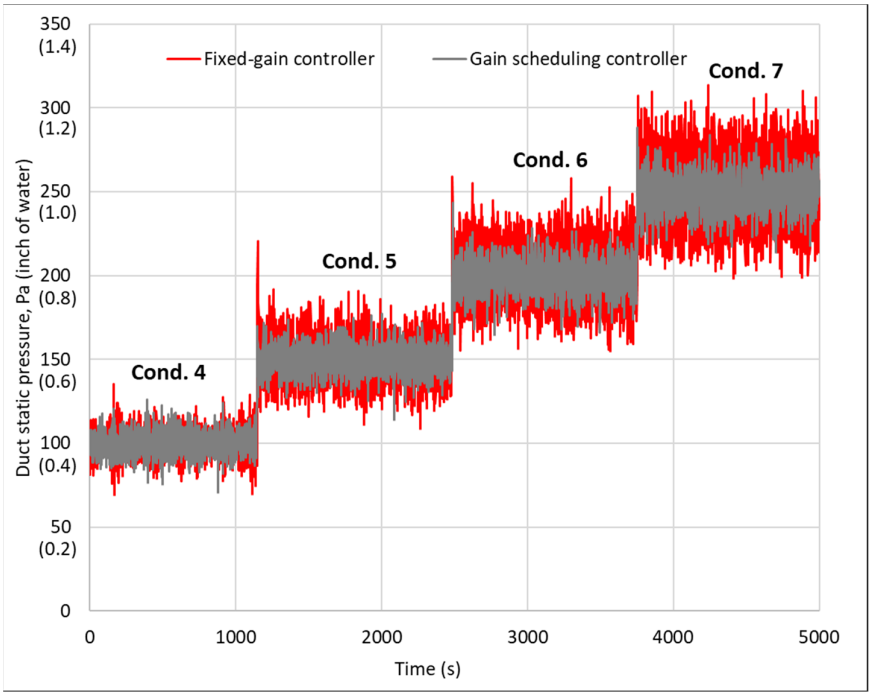

(b) System response of duct static pressure.

Fig. 12. System response with variable duct static pressure using the fixed-gain controller and gain scheduling controller.

The oscillation range of the fan speed and duct static pressure as well as the RMSE of the duct static pressure with the gain scheduling controller are also calculated and listed in Table 3. Compared to the control performance with the fixed-gain controller, under the same operation condition at the Test condition 7 with the gain scheduling controller, the oscillation range of the fan speed is 0.9Hz, which is reduced by 81%, while the oscillation range of the duct static pressure is 25 Pa (0.10 inch of water), which is reduced by 74%. The RMSE of the duct static pressure is 11 Pa (0.043 inch of water), which is 44% of that with the fixed-gain controller.

Specifically, it can be observed that the system with the gain scheduling controller does not exactly stay the same as the control performance independent of the operation conditions. Ideally, the fan-duct gain is two times that of the ratio of the duct static pressure to the fan speed, based on which the gain scheduling controller is designed. However, the tested space is a small part of a large building which is served by several large AHUs without a return fan and relief duct, and these AHUs were under economizer operation during the tests. Thus, the space static pressure was much larger than the recommended value. Consequently, the equivalent system gain varies slightly under various operation conditions. However, in practice, the space static pressure is expected to be small and the gain scheduling control strategy can achieve a critical improvement in the nonlinear control performance of the fan speed control system, which is simple and costless to implement.

6. Conclusion

A control-oriented model of the fan speed control system at AHUs has been developed and calibrated. The model reveals a nonlinear feature of the fan speed control system under normal operation where the fan duct gain is proportional to the ratio of the duct static pressure to the fan speed, which is more effective in identifying the system nonlinearities rather than the fan airflow rate.

The nonlinear feature makes the system have more aggressive control performance under the operation conditions, such as the reduced airflow rate under the fixed duct static pressure and the increased duct static pressure with the same airflow rate, where the ratio of the duct static pressure to the fan speed is larger. Specifically, the system with the fixed-gain controller under the worst operation condition, with fan speed at 50 Hz and duct static pressure at 249 Pa (1.0 inch of water), had an oscillation range of the fan speed and duct static pressure of 4.7 Hz and 69 Pa (0.28 inch of water), respectively. The RMSE of the duct static pressure was 24 Pa (0.098 inch of water).

The designed gain scheduling controller can effectively compensate for the system gain variation and approximately maintain the identical control behaviors under variable operation conditions. By applying the gain scheduling controller, the oscillation range under the same operation condition can be reduced by up to 74% for the duct static pressure and by up to 81% for the fan speed. In addition, the RMSE of the duct static pressure can also be reduced by 24 Pa (0.043 inch of water).

The contribution of this paper can be concluded as follows:

(1) The developed control-oriented model can represent the fan speed control system nonlinear characteristic while being simple enough without requiring detailed information on the system

parameters, which can be used for more effective design of duct static pressure setpoint reset control and VAV system controls.

(2) Since the derivation of the fan-duct model is based on the affinity laws, the control-oriented model can also be extended to the pump-pipe systems for better pump speed control system design.

(3) The gain scheduling control strategy can achieve almost identical fan speed control behaviors under all operation conditions.

(4) For implementation, the gain scheduling control strategy selected the readily available duct static pressure and fan speed as the scheduling variables, which is costless without additional measurements and simple enough without requiring multiple controller tuning processes.

Nomenclature

CO = VFD frequency command

D = disturbance input

H = pressure (Pa, inch of water)

I = integral

K = gain (%/Pa (%/inch of water), Hz/%, Pa/Hz (inch of water/Hz))

G = transfer function

N = fan speed (Hz)

P = proportional

r = reference condition

R = reference input

S = resistance coefficient (Pa/(L/s)^2, inch of water/CFM^2)

α, β = ratio

τ = time constant (s)

Subscripts and superscripts:

C = controller

d = design

fd = fan-duct

j = jth sample

n = total number of samples

sp = static pressure

TB = terminal box

Vm = VFD-motor

Acknowledgments

This material is based upon work supported by the U.S. Department of Energy's Office of Energy Efficiency and Renewable Energy (EERE) under the Building Technologies Office, Award Number DE-EE0008683.

Disclaimer

The views expressed herein do not necessarily represent the views of the U.S. Department of Energy or the United States Government.

Reference

Afram, A. and F. Janabi-Sharifi (2014). "Theory and applications of HVAC control systems–A review of model predictive control (MPC)." Building and Environment **72**: 343-355.

ASHRAE (2007). 2007 ASHRAE Handbook—HVAC Applications, Chapter 46, American Society of Heating, Refrigerating and Air-Conditioning Engineers ….

ASHRAE (2010). ANSI/ASHRAE/IESNA Standard 90.1-2010: Energy Standard for Buildings Except Low-Rise Residential Buildings. American Society of Heating, Refrigerating and Air-conditioning Engineers, Inc. **ISSN 1041-2336**.

Barbosa, G. C., R. Bertolin, P. J. González, A. B. Guimaraes Neto and F. J. Silvestre (2018). Fuzzy gain-scheduling applied for a very flexible aircraft. 2018 AIAA Guidance, Navigation, and Control Conference.

Chintala, R., C. Price, S. Liang and B. P. Rasmussen (2015). "Identification and Elimination of Hunting Behavior in HVAC Systems." ASHRAE Transactions **121**(2).

DOE, U. S. (2011). Buildings Energy Data Book, Energy Efficiency and Renewable Energy Department, Washington DC.

Eltayeb, A., M. F. Rahmat, M. M. Eltoum and M. A. M. Basri (2019). Adaptive fuzzy gain scheduling sliding mode control for quadrotor UAV systems. 2019 8th International Conference on Modeling Simulation and Applied Optimization (ICMSAO), IEEE.

Esrafilian-Najafabadi, M. and F. Haghighat (2021). "Occupancy-based HVAC control systems in buildings: A state-of-the-art review." Building and Environment: 107810.

Gallego, A. J., G. M. Merello, M. Berenguel and E. F. Camacho (2019). "Gain-scheduling model predictive control of a Fresnel collector field." Control Engineering Practice **82**: 1-13.

Ghefiri, K., I. Garrido, A. J. Garrido, S. Bouallègue and J. Haggège (2018). Fuzzy gain scheduling of a rotational speed control for a tidal stream generator. 2018 International Symposium on Power Electronics, Electrical Drives, Automation and Motion (SPEEDAM), IEEE.

Hao, H., Y. Lin, A. S. Kowli, P. Barooah and S. Meyn (2014). "Ancillary service to the grid through control of fans in commercial building HVAC systems." IEEE Transactions on smart grid **5**(4): 2066-2074.

Joo, I.-S., M. Liu and G. Liu (2007). "Application of fan airflow stations in air-handling units." Energy engineering **104**(2): 66-80.

Lennart, L. (1999). "System identification: theory for the user." PTR Prentice Hall, Upper Saddle River, NJ **28**.

Mei, L. and G. Levermore (2000). "Stability analysis for a VAV test rig." Building Services Engineering Research and Technology **21**(4): 225-232.

Mei, L. and G. Levermore (2002). "Simulation and validation of a VAV system with an ANN fan model and a non-linear VAV box model." Building and Environment **37**(3): 277-284.

Moradi, H., M. Saffar-Avval and F. Bakhtiari-Nejad (2011). "Nonlinear multivariable control and performance analysis of an air-handling unit." Energy and Buildings **43**(4): 805-813.

Naus, G. (2009). "Gain scheduling robust design and automated tuning of automotive controllers." TU Eindhoven.

Nise, N. S. (2019). Control Systems Engineering, 8th Edition, Wiley.

Okochi, G. S. and Y. Yao (2016). "A review of recent developments and technological advancements of variable-air-volume (VAV) air-conditioning systems." Renewable and Sustainable Energy Reviews **59**: 784-817.

Price, C. and B. Rasmussen (2015). "HVAC nonlinearity compensation using cascaded control architectures." ASHRAE Transactions **121**: 217.

Raisoni, R., N. S. Raman, P. Barooah, J. D. Munk and P. Im (2018). A control-oriented dynamic model of air flow in a single duct HVAC, Oak Ridge National Lab.(ORNL), Oak Ridge, TN (United States).

Shim, G., L. Song and G. Wang (2014). "Comparison of different fan control strategies on a variable air volume systems through simulations and experiments." Building and Environment **72**: 212-222.

Shin, Y., Y. S. Chang and Y. Kim (2002). "Controller design for a real-time air handling unit." Control Engineering Practice **10**(5): 511-518.

Singhal, A. and T. I. Salsbury (2007). "Characterization and Cancellation of Static Nonlinearity in HVAC Systems." ASHRAE Transactions **113**(1).

Tahersima, F., J. Stoustrup and H. Rasmussen (2013). "An analytical solution for stability-performance dilemma of hydronic radiators." Energy and Buildings **64**: 439-446.

Taylor, S. T. (2007). "VAV system static pressure setpoint reset." ASHRAE journal **6**.

Underwood, C. P. (2002). HVAC Control Systems: Modelling, Analysis and Design, Routledge.

Wang, J. and Y. Wang (2008). "Performance improvement of VAV air conditioning system through feedforward compensation decoupling and genetic algorithm." Applied Thermal Engineering **28**(5-6): 566-574.

Wu, Z., D. Li, Y. Xue and Y. Chen (2019). "Gain scheduling design based on active disturbance rejection control for thermal power plant under full operating conditions." Energy **185**: 744-762.

Yang, Y. and Y. Yan (2016). "Attitude regulation for unmanned quadrotors using adaptive fuzzy gain-scheduling sliding mode control." Aerospace Science and Technology **54**: 208-217.

Yueneng, Y. and Y. Ye (2018). "Backstepping sliding mode control for uncertain strict-feedback nonlinear systems using neural-network-based adaptive gain scheduling." Journal of Systems Engineering and Electronics **29**(3): 580-586.

Zaheer-Uddin, M. and G. Zheng (1994). "A VAV system model for simulation of energy management control functions: off normal operation and duty cycling." Energy Conversion and Management **35**(11): 917-931.

Zhou, X., N. Harberl and H. Cheng (2017). Demonstration of Energy Savings in Commercial Buildings for Tiered Trim and Respond Method in Resetting Static Pressure for VAV Systems, Iowa State University Ames United States.